THE JOURNAL OF BIOLOGICAL CHEMISTRY
Vol. 275, No. 22, Issue of June 2, pp. 16650–16657, 2000

Printed in U.S.A.

TASK-3, a Novel Tandem Pore Domain Acid-sensitive K^+ Channel

AN EXTRACELLULAR HISTIDINE AS pH SENSOR*

Received for publication, January 6, 2000, and in revised form March 24, 2000
Published, JBC Papers in Press, March 27, 2000, DOI 10.1074/jbc.M000030200

Sindhu Rajan‡, Erhard Wischmeyer§, Gong Xin Liu‡, Regina Preisig-Müller‡, Jürgen Daut‡¶, Andreas Karschin§, and Christian Derst‡

From the ‡Institut für Normale und Pathologische Physiologie, Marburg University, 35037 Marburg, Germany and the §Department of Molecular Neurobiology of Signal Transduction, Max-Planck-Institut für Biophysikalische Chemie, 37070 Göttingen, Germany

Tandem pore domain acid-sensitive K^+ channel 3 (TASK-3) is a new member of the tandem pore domain potassium channel family. A cDNA encoding a 365-amino acid polypeptide with four putative transmembrane segments and two pore regions was isolated from guinea pig brain. An orthologous sequence was cloned from a human genomic library. Although TASK-3 is 62% identical to TASK-1, the cytosolic C-terminal sequence is only weakly conserved. Analysis of the gene structure identified an intron within the conserved GYG motif of the first pore region. Reverse transcriptase-polymerase chain reaction analysis showed strong expression in brain but very weak mRNA levels in other tissues. Cell-attached patch-clamp recordings of TASK-3 expressed in HEK293 cells showed that the single channel current-voltage relation was inwardly rectifying, and open probability increased markedly with depolarization. Removal of external divalent cations increased the mean single channel current measured at −100 mV from −2.3 to −5.8 pA. Expression of TASK-3 in *Xenopus* oocytes revealed an outwardly rectifying K^+ current that was strongly decreased in the presence of lower extracellular pH. Substitution of the histidine residue His-98 by asparagine or tyrosine abolished pH sensitivity. This histidine, which is located at the outer part of the pore adjacent to the selectivity filter, may be an essential component of the extracellular pH sensor.

Mammalian tandem pore domain potassium channels (2P K^+ channels) contain four transmembrane regions (M1 to M4) and two pore-forming domains (P1 and P2) in each subunit (1). It is believed that two subunits dimerize to form a K^+-selective pore. So far, eight members of this gene family, denoted *KCNK*1–8, have been identified in mammals (1–7). Approximately 60 structurally related subunits of this family have been identified in the genome of the nematode *Caenorhabditis elegans* (8, 9) and at least one subunit is found in *Drosophila melanogaster* (10) and in the plant *Arabidopsis thaliana* (11). A slightly different 2P K^+ channel motif with 6 + 2 transmembrane regions has been described in the TOK1/DUK1 subunit of the budding yeast *Saccharomyces cerevisiae* (12).

Those 2P K^+ channels that functionally express in heterologous systems (but see 2, 13) generate instantaneous, noninactivating, and weakly rectifying K^+-selective currents with no apparent voltage sensitivity of activation. Thus, together with their wide distribution in various tissues they may contribute to background currents that set the membrane potential near the K^+ equilibrium potential. 2P K^+ channels are subject to modulation by a wide variety of stimuli. TREK-1 (*KCNK*2) and TRAAK (*KCNK*4) channels are mechanosensitive and are activated by arachidonic acids and other unsaturated fatty acids (14, 15). TREK-1 is, in addition, inhibited by protein kinase A and C and activated by intracellular acidification (14). The reduction in intracellular pH occurring during ischemia is expected to cause hyperpolarization and subsequent reduction of Ca^{2+} influx through voltage-activated Ca^{2+} channels. Thus, TREK-1 may play a protective role during ischemia by reducing Ca^{2+} overload (15).

TWIK-1 (*KCNK*1) and TWIK-2 (*KCNK*6) form weakly, inwardly rectifying potassium channels that are inhibited by protein kinase C and internal acidification (1, 4). It should be noted, however, that several reports showed that expression of TWIK-1 or TWIK-2 subunits alone did not produce functional channels (13, 16). Although not strongly related at the amino acid level, both TASK-1[1] (*KCNK*3) and TASK-2 (*KCNK*5) are sensitive to changes in extracellular pH (3, 6). Furthermore, TASK-1 and TREK-1 are potential targets for volatile anesthetics (17, 18).

2P K^+ channels have been found in many different tissues and are particularly abundant in the brain (except TASK-2). Here we describe the cloning and expression of a novel mammalian 2P K^+ channel, TASK-3, that is exclusively expressed in the brain. The close sequence similarity between TASK-1 and TASK-3 and the similar functional properties suggest that TASK-3 and TASK-1 may form a subfamily within the 2P K^+ channels. TASK-3, like TASK-1, is sensitive to extracellular pH and shares two extracellular histidine residues with TASK-1. Using site-directed mutagenesis we identified the histidine at position 98 near the pore selectivity filter as a component of the pH sensor.

* This work was supported in part by Deutsche Forschungsgemeinschaft Grants Da177/7-2 and Ka1175/1-2, by the Ernst und Berta Grimmke Stiftung, and by the P. E. Kempkes Stiftung. The costs of publication of this article were defrayed in part by the payment of page charges. This article must therefore be hereby marked "*advertisement*" in accordance with 18 U.S.C. Section 1734 solely to indicate this fact.

The nucleotide sequence(s) reported in this paper has been submitted to the GenBank™/EBI Data Bank with accession number(s) AF212827, AF212828, and AF212829 (for guinea pig and human TASK-3 channel cDNA).

¶ To whom correspondence should be addressed: Inst. of Physiology, Marburg University, Deutschhausstrasse 2, 35037 Marburg, Germany. Tel.: 49-6421-2866494; Fax: 49-6421-2868960; E-mail: daut@mailer.uni-marburg.de.

[1] The abbreviations used are: TASK, tandem pore domain acid-sensitive K^+ channel; RACE, rapid amplification of cDNA ends, PCR, polymerase chain reaction; 2P K^+ channel, tandem pore domain potassium channel; h, human; HEK cells, human embryonic kidney cells; NP_o, the number of channels in a membrane patch multiplied with the open probability of individual channels.

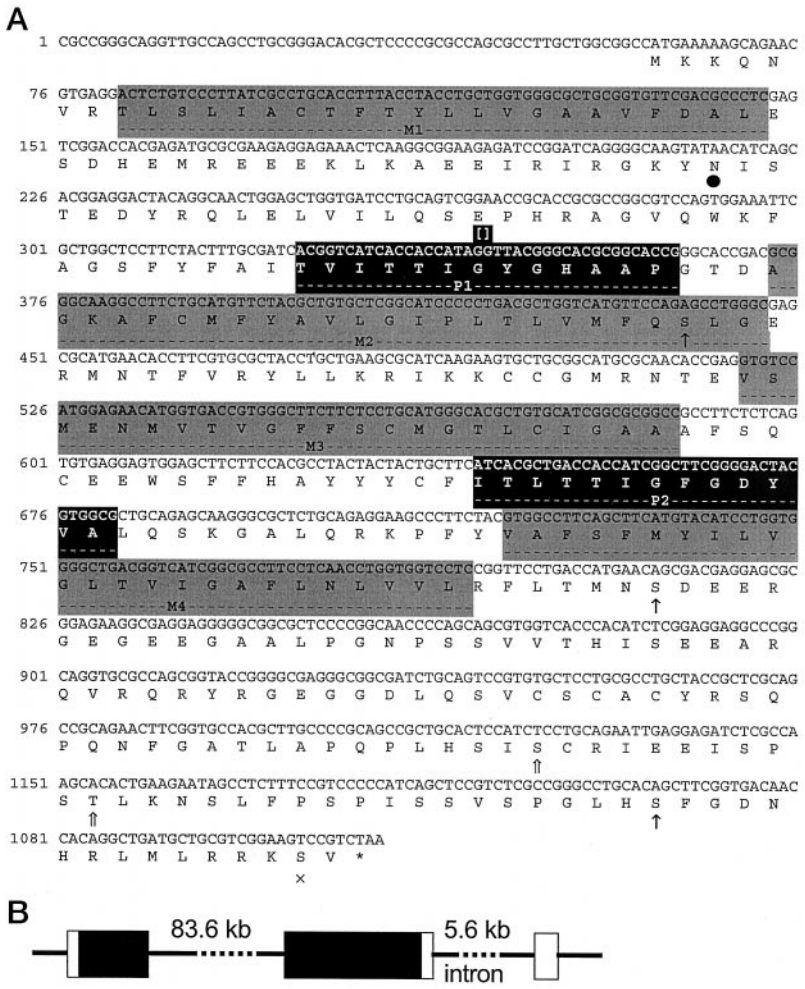

FIG. 1. **Sequence analysis of TASK-3 channels.** *A*, nucleotide and deduced amino acid sequence of guinea pig TASK-3. The positions of the transmembrane regions (*gray*) and the pore-forming regions (*black*) are indicated. Intracellular consensus phosphorylation sites for protein kinase C (⇑), cAMP-dependent protein kinase (×), and casein kinase (↑) are marked. The putative extracellular *N*-glycosylation site is labeled with a *black dot*. Consensus sites were identified using the program PROSITE. The position of the identified intron is marked by *brackets*. *B*, genomic structure of the human TASK-3 gene predicted by comparing hTASK-3 cDNA sequence, expressed sequence tag clone AA349574, and a genomic sequence from chromosome 8 (GenBank™ accession number AC007869). Exons are represented by *boxes*, and coding regions are shown in *black*. *kb*, kilobase.

EXPERIMENTAL PROCEDURES

Molecular Cloning of Guinea Pig and Human TASK-3—An expressed sequence tag clone encoding a partial sequence of mouse TASK-1 (IMAGE clone Id: IMAGp998G04768, GenBank™ accession number W36852, kindly provided by the Resource Center of the German Human Genome Project, Max-Planck-Institute for Molecular Genetics, Berlin) was labeled with digoxigenin (Roche Diagnostics, Mannheim, Germany) and used for screening of a guinea pig genomic λFIXII library of 600,000 plaque forming units (Stratagene, La Jolla, CA). Screening at reduced stringency (37 °C hybridization, 60 °C wash) resulted in the isolation of three independent λ-clones (two encoding the gpTASK-1 gene, one containing the C-terminal exon of a novel TASK-like gene, GenBank™ accession number AF212828). Two further screenings were done to purify the phages. λ-DNA was prepared using a λ-DNA Midi Kit (Qiagen, Hilden, Germany). Several restriction fragments of the DNA were subcloned and sequenced.

To obtain the entire open reading frame of gpTASK-3, a 5′-RACE of guinea pig brain poly(A)$^+$ cDNA was performed using the Marathon cDNA Amplification Kit (CLONTECH, Palo Alto, CA). For this nested PCR approach, two gene-specific primers (5′-CTCCATGGACACCTCG GTGTTGCG-3′ and 5′-AGAACATGCAGAAGGCCTTGCCCG-3′) and two adapter primers (AP1 and AP2, see kit) were used to amplify the 5′-end of the gpTASK-3 cDNA using a touchdown PCR protocol and the Advantage cDNA polymerase mixture (CLONTECH) as described by the manufacturer. The RACE product was directly sequenced with flanking primers.

Screening of 500,000 plaque forming units of a human λ-DASH library (Stratagene) using a gpTASK-3-specific DNA fragment isolated five independent genomic clones. After purifying λ-DNA as described above, the clones were directly sequenced. For sequence analysis the GCG program package implemented at the Heidelberg Unix Sequence Analysis Resources was used.

Expression Vectors and Mutagenesis of TASK-3—To amplify the entire gpTASK-3 open reading frame from guinea pig brain cDNA, two primers containing the start/stop codon and *Bam*HI/*Eco*RI restriction sites (shown in *italics*) were designed: forward, 5′-GCTG*GGATCC*ATGAAAAAGCAGAACGTGAG-3′ and back, 5′-CTCC*GAATTC*TTAGACGGACTTCCGACGCAG-3′. The coding region of hTASK-3 was amplified from a human whole-brain Marathon-Ready cDNA (CLONTECH) using similar primers: forward, 5′-GCTG*GGATCC*ATGAAGAGGCAGA ACGTG-3′ and back, 5′-TCCC*GAATTC*TAAACGGACTTCCGGCGT-3′. The PCR-fragments were cloned into the expression vector pSGEM (a kind gift of Dr. M. Hollmann) and into pcDNA3.1(+) (Invitrogen, Leek, The Netherlands). For mutagenesis of gpTASK-3 cDNA the Quik Change site-directed mutagenesis kit (Stratagene) was used. 31-mer oligonucleotides were designed with 15 annealing bases on each side of the intended base change. The first position of the codon for His-72, His-98, and His-188 was changed from C to G, A, or T. After random sequencing of ten clones for each mutagenesis reaction the following mutations were obtained and electrophysiologically characterized: H72D, H72Y, H98Y, H98N, H188D, H188Y, and H188N.

Tissue Distribution Using Reverse Transcriptase-PCR—RNA from several tissues of guinea pig was extracted using a modified acid guanidinium method (19) and reverse transcribed with Superscript II Reverse Transcriptase (Life Technologies, Inc.). Gene-specific and intron-spanning primers (forward, 5′-GCAAGTATAACATCAGCACGGA-3′ and back, 5′-GAAGAAGCTCCACTCCTCACAC-3′) were used to selectively amplify a 413-base pair fragment of gpTASK-3 cDNA. PCR products were analyzed on a 4% Nusieve agarose gel.

Single Channel Recording in HEK293 Cells—HEK293 cells were cultured at a density of ~2 × 10^5/35-mm dish and transfected with 0.6–1 μg of gpTASK-3 in the pcDNA3.1(+) vector, using LipofectAMINE (Life Technologies, Inc.) according to the manufacturer's protocol. Cell-attached single channel currents were recorded using an EPC-7 patch clamp amplifier (List, Darmstadt, Germany). The pipette resistance was in the range of 8–12 megaohms. The normal pipette solution contained: 145 mM KCl, 1 mM $CaCl_2$, 1 mM $MgCl_2$, 5 mM HEPES; the pH was adjusted to 7.4 with KOH. The divalent-free pipette solution was prepared from a solution containing 132 mM KCl, 5 mM EGTA, and 5 mM HEPES; the pH was adjusted by adding KOH to

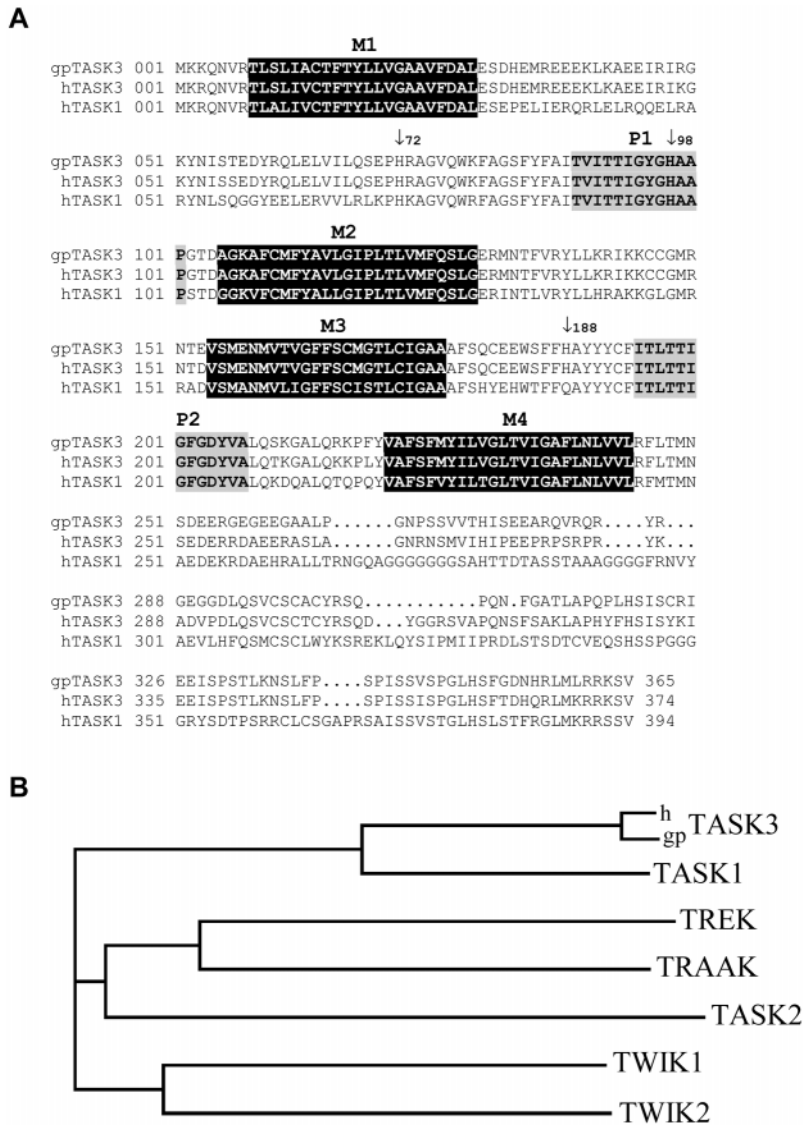

FIG. 2. **Sequence comparison of gpTASK-3.** *A*, sequence alignment of human and guinea pig TASK-3 and human TASK-1 cDNA. Transmembrane regions and pore-forming regions are marked by *black* and *gray boxes*, respectively. *Arrows* denote the extracellular histidine residues addressed in the mutation analysis. Calculations were performed with the program CLUSTAL W (HUSAR). *B*, phylogenetic tree of seven mammalian 2P K^+ channels (GenBank™ accession numbers: human TASK-1, AF006823; human TREK-1, AF129399; mouse TRAAK, AF056492; human TASK-2, AF084830; human TWIK-1, U33632; human TWIK-2, AF117708). The CLUSTAL/CLUSTREE algorithm (Heidelberg Unix Sequence Analysis Resources) was used for computation.

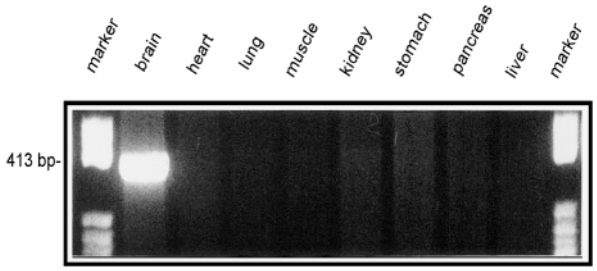

FIG. 3. **Tissue localization of gpTASK-3 using reverse transcriptase-PCR.** Reverse-transcribed cDNA from the tissues indicated was analyzed for the presence of a 413-base pair (*bp*) PCR fragment. The *left lane* shows a pBR322/*Hae*III marker.

pH 7.4. The estimated final K^+ concentration of both solutions was 150 mM. The bath solution contained: 140 mM KCl, 2 mM $MgCl_2$, 5 mM HEPES, 10 mM glucose; the pH was adjusted to 7.4 with NaOH. Data were acquired using pClamp7 software and analyzed using a software developed in our laboratory (P.C.DAQ 1.0) using LabView (National Instruments). The sampling frequency was 2.5 kHz for voltage step protocols and 10 kHz for gap-free continuous recording; the −3 dB cut-off frequency was 0.5 and 2 kHz, respectively.

Whole-cell Recording of TASK-3 Currents in Xenopus Oocytes—Capped run-off poly(A)$^+$ cRNA transcripts from linearized gpTASK-3 cDNA (wild type and mutants) were synthesized, and about 6 ng were micro-injected into each defolliculated oocyte. Oocytes were incubated at 20 °C in ND96 solution (96 mM NaCl, 2 mM KCl, 1 mM $MgCl_2$, 1 mM $CaCl_2$, 5 mM HEPES, pH 7.4) supplemented with 100 μg/ml gentamicin and 2.5 mM sodium pyruvate. 48 h after injection, two-electrode voltage-clamp measurements were performed with a TURBO TEC-10 C amplifier (npi, Tamm, Germany), and currents were recorded with an EPC9 patch-clamp amplifier (Heka Electronics, Lambrecht, Germany). Stimulation and data acquisition were controlled by PULSE/PULSEFIT software (Heka). Oocytes were placed in a small volume perfusion chamber with a constant flow of ND96 solution or high K^+ solution (96 mM KCl, 2 mM NaCl, 1 mM $MgCl_2$, 1 mM $CaCl_2$, 5 mM HEPES) titrated to different pH with NaOH. Data are presented as mean ± S.D.; *n* indicates the number of cells.

RESULTS

Sequence Analysis of Guinea Pig and Human TASK-3—Sequence analysis of genomic and 5′-RACE clones isolated from guinea pig identified a putative open reading frame of 1095-base pairs encoding 365 amino acids (Fig. 1*A*, GenBank™ accession number AF212827). Hydrophobicity analysis of the primary sequence using the algorithm of Kyte and Doolittle (20) showed the typical organization of a 2P K^+ channel with four transmembrane segments and two independent pore-forming regions containing the TXG(YIF)G consensus motif of potassium channels (Fig. 1*A*). A large extracellular loop of 60 amino acids is present between M1 and P1. Whereas only six amino acids precede M1, the sequence harbors a cytosolic C terminus of 121 amino acids containing two consensus protein kinase C phosphorylation sites, two casein kinase phosphoryl-

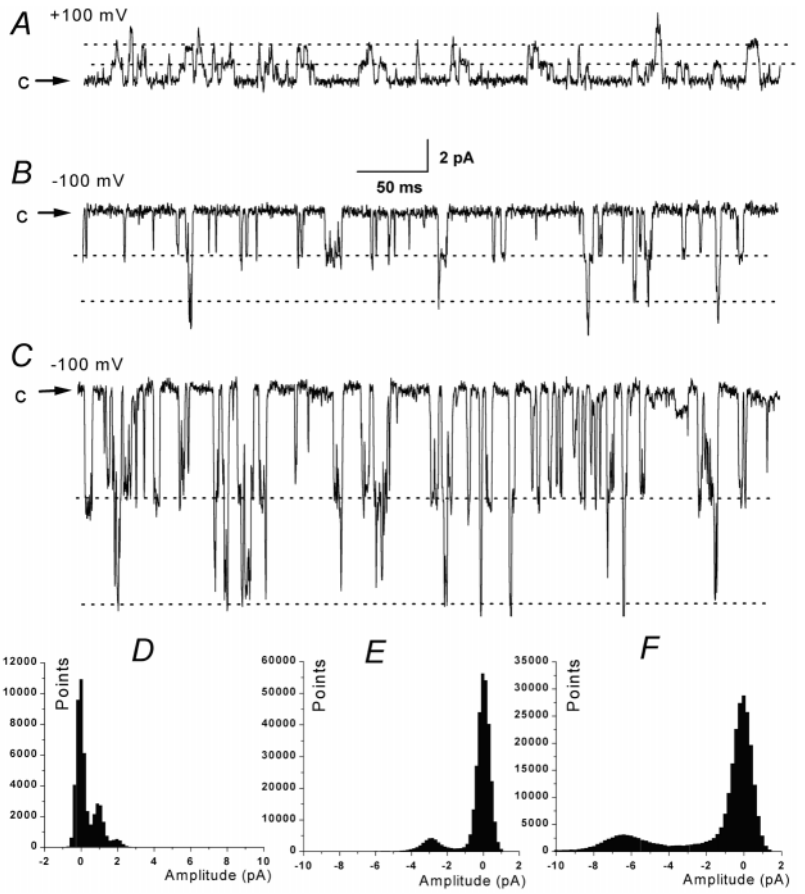

FIG. 4. **TASK-3 channels expressed in HEK293 cells.** *A*, typical cell-attached recording of TASK-3 channels expressed in HEK293 cells. Gap-free recordings lasting at least 30 s were performed at membrane potentials of +100 and −100 mV (inside-outside). Outward current is upward, the closed state (*c*) is indicated by an *arrow*, and the open states are indicated by *dotted lines*. In tracks *A* and *B*, the pipette solution contained 1 mM Ca^{2+} plus 1 mM Mg^{2+}. In *C*, divalent cations were omitted. The point-amplitude histograms corresponding to *A*, *B,* and *C* are shown in *D*, *E,* and *F*. The bin width was 0.1 pA.

ation sites, a cAMP-dependent protein kinase phosphorylation site, and a conserved region showing homology to the TASK-1 PDZ-binding motif. However, the PDZ consensus motif found in TASK-1 (RSSV-Stop) is not conserved in TASK-3 (RKSV-Stop). Because of the sequence similarity to TASK-1 (6) and the physiological properties of the channel (see below), we named this channel subunit TASK-3.

Sequence comparison (Fig. 2*A*) shows that gpTASK-3 is closely related to TASK-1 with 62.3% overall identity. Homology to other 2P K^+ channels is low with only 25–30% identity. Sequence identity to TASK-1 is much higher in the core region comprising transmembrane regions, extracellular loops and pore regions (74.4%), than in the C-terminal part (33.9%). Phylogenetic analysis showed that TASK-1 and TASK-3 (but not TASK-2) form an independent cluster among 2P K^+ channels and may represent the first two members of a subfamily (Fig. 2*B*). Two further structural features support this hypothesis: First, the sequences at the extreme C terminus are conserved between TASK-1 and TASK-3, but show no significant homology to other 2P K^+ channels. Second, TASK-1 and TASK-3 lack an extracellular cysteine residue in the M1-P1 loop, which is conserved in other 2P K^+ channels and may covalently link the subunits in dimeric channels (21). Instead, both TASK subunits have an *N*-glycosylation site at the equivalent position.

To identify the human ortholog of gpTASK-3 (hTASK-3) we screened a human genomic library and isolated five independent clones showing sequence identity to a recently released DNA fragment of chromosome 8 (locus D8S1741, AC007869). Analysis of the entire data base entry revealed the presence of a 83.6-kilobase intron splitting the hTASK-3 open reading frame at the first glycine of the GYG motif of P1. This position is conserved in most of the 2P K^+ channels of *C. elegans* (8) and in the gpTASK-3 gene (GenBank™ accession number AF212828). Furthermore, a human infant brain expressed sequence tag clone (GenBank™ accession number AA349574) encoding a partial hTASK-3 cDNA revealed a second 5.6-kilobase intron in the 3′-nontranslated region (Fig. 1*B*). The deduced hTASK-3 open reading frame encodes 374 amino acids (GenBank™ accession number AF212829), and is 88.3% identical to gpTASK-3 at the amino acid level. Whereas the core regions of hTASK-3 and gpTASK-3 are nearly identical (96.8%), the C-terminal parts showed significantly lower homology (69.8% identity).

Tissue Distribution of gpTASK-3—To determine the tissue distribution of TASK-3, a specific 413-base pairs fragment was amplified from different guinea pig RNA samples by reverse transcriptase-PCR. Intron-spanning primers were designed to exclude false positive signals resulting from possible genomic DNA contamination. Strong expression was detected exclusively in the brain (Fig. 3). With prolonged PCR cycling (up to 80 cycles) weak signals also appeared in other tissues, especially in the kidney (data not shown). It is not yet clear whether this weak expression is of neuronal origin, for example peripheral parasympathetic ganglia.

Elementary Properties of the gpTASK-3 Channel Expressed in HEK293 Cells—gpTASK-3 channels were expressed in HEK293 cells and studied in the cell-attached mode of the patch-clamp technique. The bath solution contained 140 mM K^+ to depolarize the cells to ~0 mV. Fig. 4 shows typical records taken at membrane potentials (inside-outside) of −100 and +100 mV and the corresponding point-amplitude histograms (Fig. 4, *D* and *E*). The pipette solution in this experiment contained 2 mM divalent cations (1 mM Ca^{2+} plus 1 mM Mg^{2+}) in addition to 150 mM K^+.

The mean single channel current was −2.30 ± 0.23 pA (n = 15) at −100 mV and +0.99 ± 0.13 pA (n = 9) at +100 mV. All records contained two or more channels with the same ampli-

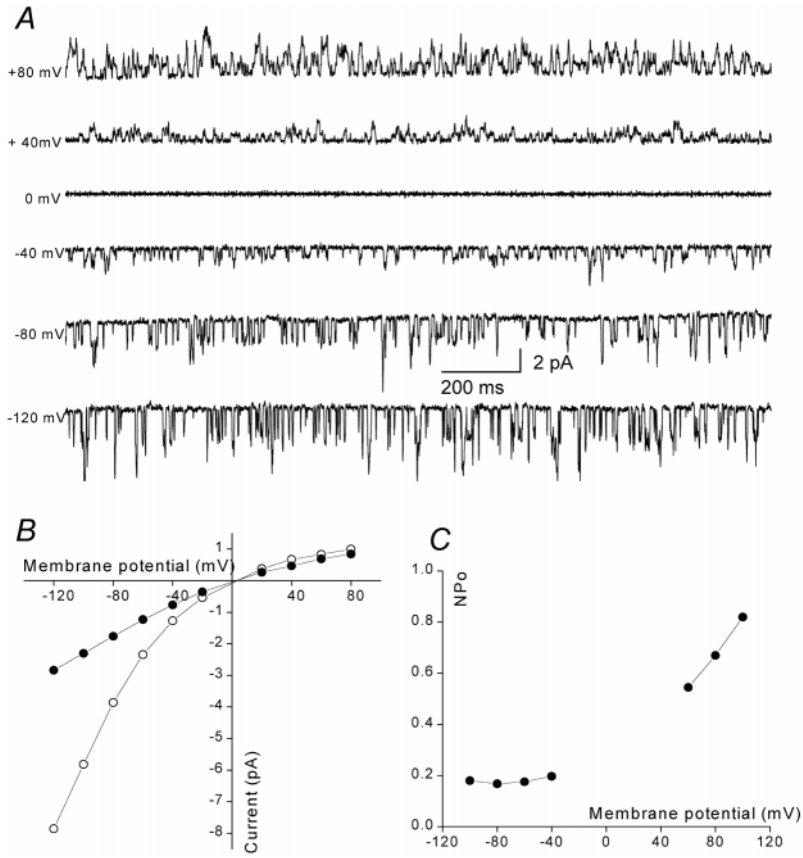

FIG. 5. **Voltage dependence of single channel amplitude and open probability.** *A*, typical cell-attached recording with a pipette solution containing 1 mM Ca^{2+} and 1 mM Mg^{2+}. Successive voltage steps of a 2.2-s duration were applied from a holding potential of 0 mV to potentials between −120 to +100 mV. Smaller, but more frequent openings were observed at positive potentials. *B*, single channel current-voltage relation with (*filled circles*) and without (*open circles*) divalent cations in the pipette solution. The mean values of at least 15 experiments are plotted. *C*, dependence of $N P_o$ on membrane potential determined in the presence of external divalent cations. Multiplying the single channel current voltage relation of TASK-3 (*C*) with $N P_o$ gives a current-voltage relation with weak outward rectification similar to the macroscopic whole-cell current voltage relation at symmetrical K^+ concentration shown in Fig. 6*C* (*lowermost trace*).

tude. When divalent cations were omitted from the pipette solution (Fig. 4, *C* and *F*), the difference in amplitude between inward and outward currents was even more pronounced. The mean single channel (outward) current at +100 mV was nearly unchanged (+1.04 ± 0.04 pA; $n = 4$), whereas the inward current at −100 mV (−5.8 ± 0.4 pA; $n = 16$) was about twice as large as in the presence of external divalent cations. Control measurements in nontransfected cells with normal pipette solution (1 mM Ca^{2+}, 1 mM Mg^{2+}, $n = 25$) or with Ca^{2+}- and Mg^{2+}-free pipette solution ($n = 10$) showed no such K^+ channels. In another series of control experiments in which HEK293 cells were transfected with Kir2.2 channel cDNA using the same vector ($n = 16$), single channel openings at positive potentials were only rarely observed. Thus, under our recording conditions a contribution of endogenous channels to the single channel currents observed after transfection with TASK-3 cDNA is unlikely.

Voltage steps to potentials between −120 and +80 mV were performed to obtain the complete single channel current-voltage relation of gpTASK-3 (Fig. 5*A*). The reversal potential was near 0 mV, as expected for a K^+-selective channel (Fig. 5*B*). It can be seen that with and without divalent cations the current voltage relation was nonlinear from −120 to +80 mV. Inward rectification was more pronounced in the absence of divalent cations. The slope conductance at −100 mV was 27.4 ± 2.3 pS ($n = 15$) in the presence and 100.4 ± 9.3 pS ($n = 16$) in the absence of external divalent cations. When the pH of the pipette solution was lowered to 6.2 in the presence of divalent external cations, the single channel slope conductance at −100 mV was decreased to 21.2 ± 2.0 pS ($n = 4$).

Despite the fact that all patches contained more than one channel, it was obvious that the open probability was larger at positive potentials than at negative potentials (Fig. 5*A*). To quantify this observation, we studied the dependence of $N P_o$ (the product of number of channels in the patch times the open probability) on the applied transmembrane potential (Fig. 5*C*). $N P_o$ showed little voltage dependence in the negative range but was markedly increased at positive potentials.

In the records taken in the absence of divalent external cations at −100 mV, the number of channels in the patch was estimated by comparing the fractional time during which 0, 1, 2, 3 . . . channels were open with the binomial distribution expected for identical and independent channels (22, 23). In all patches examined ($n = 8$), the number of channels/patch was estimated to be ≥10. From these data and the values of $N P_o$ (Fig. 5*C*) an upper limit for the open probability at different potentials can be derived: P_o was <0.02 in the range −100 to −40 mV and <0.1 at positive potentials.

Properties of gpTASK-3 Currents in Xenopus Oocytes—After the injection of gpTASK-3 cRNA into *Xenopus* oocytes, large outward currents were detected in the two-electrode voltage clamp. Such currents were absent in noninjected or water-injected control oocytes (Fig. 6*A*). At day 2 after injection, steady-state current amplitudes averaged 42.4 ± 14.1 μA ($n = 10$) at +30 mV in the presence of 2 mM external $[K^+]$ ($[K^+]_e$). Activation kinetics in response to depolarizing voltage pulses was not instantaneous but showed a rise time of 2–4 ms between −20 to +60 mV (Fig. 6*B*). There was no inactivation in the time period examined (up to 5 s). The steady-state current-voltage relationship determined from ramp and step protocols was outwardly rectifying, and at low $[K^+]_e$ only a little inward current could be detected (Fig. 6*C*). When ($[K^+]_e$) was altered to examine the ion selectivity of gpTASK-3, the measured zero current potentials were −93 (2 mM K^+), −68 (5 mM), −54 (10 mM), −35 (25 mM), −20 (50 mM), and −7 mV (96 mM), which agrees well with E_K as predicted from the Nernst equation (assuming internal $[K^+]$ of ~100 mM). Fig. 6*D* demonstrates that the zero current potentials followed $[K^+]_e$ with a slope of ~49 mV/decade, indicating that the conductance was predominantly carried by K^+ ions. Expression of hTASK-3 channels in

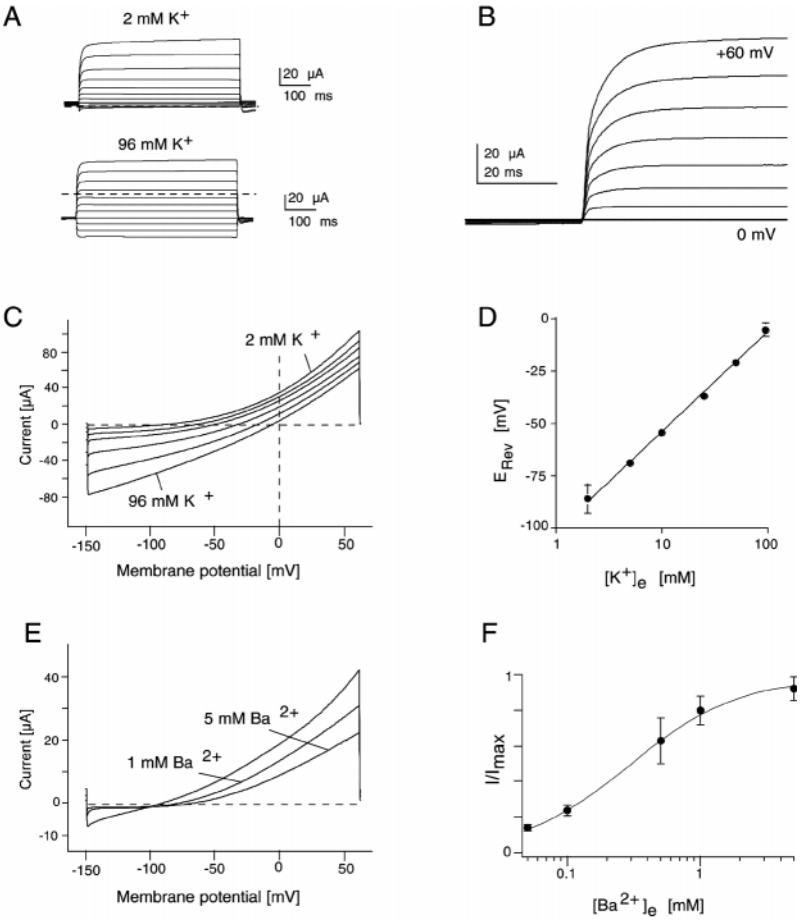

FIG. 6. **Expression of gpTASK-3 channels in *Xenopus* oocytes.** *A*, whole-cell current recordings from *Xenopus* oocytes injected with gpTASK-3 cRNA. Voltage steps of 500 ms duration to potentials between +60 and −140 mV were applied from a holding potential of −80 mV. The extracellular K^+ concentration was 2 mM in the *upper panel* and 96 mM in the *lower panel*. *B*, current activation after brief depolarizing voltage jumps reveals rise times (66.7% of I_{max}) of 3.9 (60 mV), 3.7 (40 mV), 3.4 (20 mV), 2.9 (0 mV), and 2.4 ms (−20 mV). *C*, current-voltage relations recorded at various extracellular K^+ concentrations using voltage ramps between −150 mV and +60 mV. *D*, zero current (reversal potentials) of gpTASK-3 currents are plotted *versus* $[K^+]_e$ on a semilogarithmic scale. The *solid line* represents a linear regression fit to the data. *E*, ramp current responses show the voltage dependence of TASK-3 block by 1 and 5 mM Ba^{2+}, respectively. *F*, The ratio of TASK-3 amplitudes in the presence and absence of Ba^{2+} (I/I_{max}) is plotted against the Ba^{2+} concentration for a potential of −130 mV. The least squares fit is derived from $IBa^{2+} = A/1 + ([Ba^{2+}]_e/K_i)$, where A is a variable and K_i is the Ba^{2+} concentration that causes a half-maximal block (290 µM).

Xenopus oocytes revealed currents of similar amplitude and identical properties ($n = 4$).

Our standard extracellular solution contained 1 mM Ca^{2+} and 1 mM Mg^{2+}. Removal of external Mg^{2+} increased the whole-cell inward current at −150 mV by a factor of 2.3 ± 1.1, whereas removal of external Ca^{2+} increased inward current by a factor of 2.9 ± 1.5 ($n = 8$; data not shown). To characterize gpTASK-3 channels further, the sensitivity of the whole-cell currents to Ba^{2+} and Cs^+ was tested. The IC_{50} for Ba^{2+} ions was >5 mM at +30 mV and 290 ± 8 µM ($n = 3$) at −130 mV, consistent with a low affinity voltage-dependent Ba^{2+} block. The channels were even less sensitive to Cs^+ block. Application of 10 mM Cs^+ reduced macroscopic currents by only 8–12% at +30 and −130 mV. The insensitivity of TASK-3 to blockade by Cs^+ is shared by TASK-2 (3) but not by TASK-1 (6).

It should be noted that the macroscopic TASK-3 currents measured in oocytes were consistent with the elementary TASK-3 currents measured in HEK293 cells. The outward rectification found in the whole-cell currents may be reconciled with the inward rectification of the single K^+ channels by taking into account the marked increase in open probability observed at positive potentials (Fig. 5*C*). The 23% decrease in single channel conductance observed after reduction of external pH from 7.4 to 6.2 suggests that the reduction of K^+ current observed during acidification was mainly because of a change in single channel conductance and was not associated with a major change in open probability.

The Extracellular pH Sensor—Similar to TASK-1 (6) and TASK-2 (3), TASK-3 currents were found to be highly sensitive to variations of extracellular pH. Acidification inhibited gpTASK-3 activity, and inward currents were completely and reversibly blocked at pH 4 (Fig. 7). Proton block occurred with a fast time course and appeared to be independent of membrane potential. The pH dependence of the gpTASK-3 current was described by a titration curve with a Hill coefficient of 0.5. The proton-mediated inhibition had an apparent pK of 5.96 (Fig. 6, *A* and *B*), which is almost one unit lower than in the case of TASK-1. Thus, significant changes in gpTASK-3 currents occur at a pH <7.0, which is below physiological values but well within the range observed during hypoxia.

The reduction in extracellular pH might be associated with a secondary change in intracellular pH. Therefore, the sensitivity of TASK-3 currents to intracellular pH was tested by the "rebound-acidification technique": The extracellular solution was switched for 5 min to a solution (of equal pH) to which 20 mM NH_4Cl had been added. After the removal of NH_4Cl, which is expected to elicit a transient intracellular acidification by ≈1 pH unit, no change in the amplitude of the TASK-3 current was observed ($n = 5$). These findings suggest that intracellular acidification did not affect the properties of the TASK-3 channels.

The residues responsible for the pH sensitivity of TASK-3 were investigated by constructing a series of mutants in which the titratable histidine residues in the extracellular linker regions were replaced. When expressed in oocytes, all substitution mutants at residues His-72 (H72D and H72Y) and His-188 (H188D, H188N, and H188Y) displayed pronounced pH sensitivity, indistinguishable from wild type channels. In contrast, the mutant channels H98N and H98Y showed a marked change in proton sensitivity, as can be seen from the steady-state currents and the pH titration curves (Fig. 7, *C* and *D*). The midpoint of the titration curve shifted from 5.9 (wild type) to 3.9 (H98Y) and 3.0 (H98N). These findings indicate that the titratable His-98 residue in gpTASK-3 is essential for the pH sensitivity of the potassium current carried by TASK-3 channels.

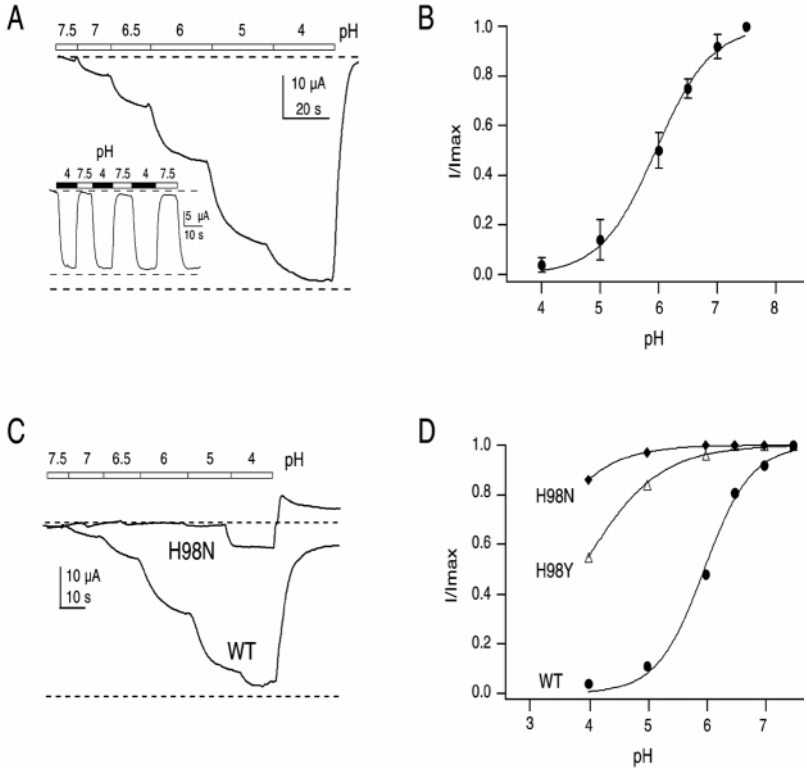

FIG. 7. **Sensitivity of wild type and mutant gpTASK-3 channels to external pH.** *A* and *C,* continuous recordings in 2 mM $[K^+]_e$ at a holding potential of +30 mV of oocytes injected with wild type gpTASK-3 cRNA (*A*) and mutant channels (*C*) in which a histidine at position 98 was replaced by an asparagine residue (H98N). *Bars* indicate application of external solutions with pH values as indicated. The *inset* recording in (*A*) illustrates the rapid reversibility of channel block by pH 4 solutions. *B* and *D*, pH titration curves wild type gpTASK-3 (*B*) and mutant gpTASK-3-H98N and gpTASK-3-H98Y (*D*). Plot of the relative amplitude of gpTASK-3 currents as compared with current amplitudes at pH 8 (I/I_{max}) against pH. Curves represent least-squares fits of the data to the Hill equation. *WT*, wild type.

DISCUSSION

TASK-3 is a new member of the family of tandem pore domain potassium channels. Sequence analysis showed that the typical structural features of previously cloned 2P K^+ channels are also found in TASK-3: (i) four conserved transmembrane regions, (ii) two pore-forming regions with a GYG(H/N/Y) motif in P1 and a G[FL]GD motif in P2, and (iii) a large extracellular M1-P1 linker region. When comparing human and guinea pig sequences it is obvious that the cytosolic part of TASK-3 channels is not strongly conserved, except for the last 26 nucleotides at the C-terminal end. Although not a typical consensus PDZ-binding motif, this region has considerable sequence homology to the TASK-1 PDZ-binding motif. Because gpTASK-3 is expressed almost exclusively in the brain, it may be speculated that this domain is important for subcellular localization in neuronal cells. Whereas some 2P K^+ channels may form covalently linked dimeric channels by connecting the M1-P1 linkers through an extracellular disulfide bridge (21), no conserved cysteine residue is found in the TASK-3 M1-P1 linker. Instead, an N-glycosylation site is found at the homologous position in TASK-3. It is not yet clear whether the glycosylation of TASK-3 is important for dimerization.

The close sequence similarity of TASK-3 and TASK-1 indicates that these two channels are the first mammalian members of a distinct subfamily of the 2P K^+ channels. The mammalian 2P K^+ channels cloned so far showed no phylogenetic clustering into subfamilies. Although some 2P K^+ channels have similar physiological properties, for example TWIK-1 and TWIK-2 or TASK-1 and TASK-2, the homology between these channels is not higher than the homology among other members of the 2P K^+ channel family. The sequences of the nematode 2P K^+ channels, however, have been shown to cluster into subfamilies (25). Phylogenetic analysis (25) shows that the nematode channels n2P38 and n2P20 also belong to the TASK-1/TASK-3 subfamily. Most of the nematode genes have introns within the codon for the first glycine residue of the P1 signature sequence GYG (21). TASK-3 also possesses an intron at this position, indicating a common ancestral gene structure.

```
1st pore                    His98
gpTASK-3  WKFAGSFYFAITVITTIGYGHAAPGTDAGK
 hTASK-1  WRFAGSFYFAITVITTIGYGHAAPSTDGGK
 hTASK-2  WNWPNAMIFAATVITTIGYGNVAPKTPAGR
 hTREK-1  WDLGSSFFFAGTVITTIGFGNISPRTEGGK
 hTWIK-1  WDFTSALFFASTVLSTTGYGHTVPLSDGGK
 hTWIK-2  WDFASALFFASTLITTVGYGYTTPLTDAGK
 mTRAAK   WNLGSAFFFSGTIITTIGYGNIVLHTDAGR

          <  pore helix  ><filter>
```

FIG. 8. **Multiple alignment of the first pore region of mammalian 2P K^+ channels. The position of His-98 is indicated. Structural features were taken from the crystal structure of the** *Streptomyces lividans* KcsA channel (24). The GenBank™ accession numbers are given in the legend of Fig. 2.

The current voltage relation of elementary TASK-3 channels was nonlinear (concave downward) in the range −120 to 0 mV, both with and without external cations, indicating that the single channel slope conductance increased with hyperpolarization in the presence of symmetrical 150 mM K^+. In this respect, TASK-3 differs from the other 2P K^+ channels such as TASK-1/TBAK (26, 27), TASK-2 (6), TRAAK (5), and also from most two-transmembrane-domain inward rectifier channels. The pronounced increase in open probability of TASK-3 with depolarization is also a novel finding. P_o of other 2P K^+ channels was reported to be independent of membrane potential (26, 29). The single channel conductance of TASK-3 was much larger in the absence of external divalent cations (from 27 to 100 pS at −100 mV). Such a dependence of single channel conductance on divalent cations has not been previously found in 2P K^+ channels.

The whole-cell currents measured in *Xenopus* oocytes injected with TASK-3 cRNA decreased with extracellular acidification, in line with the unique functional properties of TASK-1 and TASK-2. However, whereas TASK-1 and TASK-2 fully open or close within a range of 0.5 pH units (3, 6) around the physiological pH (7.3–7.8), TASK-3 is most sensitive to extracellular H^+ changes between pH 5 and 7. When His-98 of TASK-3 was changed to asparagine, the p*K* decreased from 5.9

to 3. This agrees reasonably well with the nominal p*K* values for the side chains of the free amino acids (6 and 3.9, respectively), indicating that the pH sensitivity of TASK-3 is mainly determined by His-98, the histidine at position +1 adjacent to the selectivity filter of the first P region. Unlike in TASK-1 and other potassium channels (30), the chemical environment in TASK-3 does not create a p*K* shift at this residue. The equivalent histidine residue is also present in TASK-1.

Histidine side chains have been implicated in the pH sensitivity of other K^+ channels (31, 32). However, apart from the protonation of the side chain, the mechanism underlying the pH sensitivity also depends on the electrostatic interactions defined by the tertiary structure of the individual channel subunits. This may differ considerably between various 2P K^+ channels, which complicates the analysis. For example, TWIK-1, the first identified member of 2P K^+ channel family, also harbors a histidine residue at the equivalent position in the first pore region (Fig. 8), but no pH dependence has been reported for this channel. Conversely, the corresponding position in TASK-2 is occupied by an asparagine (Fig. 8), indicating that the pH sensitivity of this subunit may be attributable to a different pH sensor site.

TASK-3 could play an important role under pathophysiological conditions. TASK-3 channels are most sensitive to pH changes in the range 7 to 6. Extracellular pH changes in this range are observed during cerebral ischemia and may depolarize the cells by inhibition of TASK-3 channels. Such a depolarization would be expected to cause an increase in the firing rate of specific neurons expressing TASK-3. This is in marked contrast to the function of other 2P K^+ channels such as TREK-1, which are activated by intracellular acidification and may have a neuroprotective function (14). The highly cell-specific pattern of expression of 2P K^+ channels in the brain (5, 7, 28) suggests that the structural diversity of these channels, especially notable in the C-terminal region and in the large M1-P1 linker region, may serve important regulatory functions in different neuronal cell types.

Acknowledgments—We thank Günter Schlichthörl and Allen Bassaly for their help in developing the single channel evaluation program, Annette Hennighausen, Dirk Reuter, Andrea Schubert, Robert Graf, Kersten Schneider, Lothar Krapp, and Antonio Mazzola for excellent technical assistance, and Erika Hoffmann for invaluable secretarial help.

REFERENCES

1. Lesage, F., Guillemare, E., Fink, M., Duprat, F., Lazdunski, M., Romey, G., and Barhanin, J. (1996) *EMBO J.* **15,** 1004–1011
2. Salinas, M., Reyes, R., Lesage, F., Fosset, M., Heurteaux, C., Romey, G., and Lazdunski, M. (1999) *J. Biol. Chem.* **274,** 11751–11760
3. Reyes, R., Duprat, F., Lesage, F., Fink, M., Salinas, M., Farman, N., and Lazdunski, M. (1998) *J. Biol. Chem.* **273,** 30863–30869
4. Chavez, R. A., Gray, A. T., Zhao, B. B., Kindler, C. H., Mazurek, M. J., Mehta, Y., Forsayeth, J. R., and Yost, C. S. (1999) *J. Biol. Chem.* **274,** 7887–7892
5. Fink, M., Lesage, F., Duprat, F., Heurteaux, C., Reyes, R., Fosset, M., and Lazdunski, M. (1998) *EMBO J.* **17,** 3297–3308
6. Duprat, F., Lesage, F., Fink, M., Reyes, R., Heurteaux, C., and Lazdunski, M. (1997) *EMBO J.* **16,** 5464–5471
7. Fink, M., Duprat, F., Lesage, F., Reyes, R., Romey, G., Heurteaux, C., and Lazdunski, M. (1996) *EMBO J.* **15,** 6854–6862
8. Wei, A., Jegla, T., and Salkoff, L. (1996) *Neuropharmacology* **35,** 805–829
9. Bargmann, C. I. (1998) *Science* **282,** 2028–2033
10. Goldstein, S. A. N., Price, L. A., Rosenthal, D. N., and Pausch, M. H. (1996) *Proc. Natl. Acad. Sci. U. S. A.* **93,** 13256–13261
11. Czempinski, K., Zimmermann, S., Ehrhardt, T., and Müller-Röber, B. (1997) *EMBO J.* **16,** 2565–2575
12. Ketchum, K. A., Joiner, W. J., Sellers, A. J., Kaczmarek, L. K., and Goldstein, S. A. N. (1995) *Nature* **376,** 690–695
13. Poutney, D. J., Gulkarov, I., Vega-Saenz de Miera, E., Holmes, D., Saganich, M., Rudy, B., Artman, M., and Coetzee, W. A. (1999) *FEBS Lett.* **450,** 191–196
14. Maingret, F., Patel, A. J., Lesage, F., Lazdunski, M., and Honoré, E. (1999) *J. Biol. Chem.* **274,** 26691–26696
15. Maingret, F., Fosset, M., Lesage, F., Lazdunski, M., and Honoré, E. (1999) *J. Biol. Chem.* **274,** 1381–1387
16. Goldstein, S. A. N., Wang, K. W., Ilan, K., and Pausch, M. H. (1998) *J. Mol. Med.* **76,** 13–20
17. Kindler, C. H., Yost, C. S., Gray, A. T. (1999) *Anesthesiology* **90,** 1092–1102
18. Patel, A. J., Honore, E., Lesage, F., Fink, M., Romey, G., and Lazdunski, M. (1999) *Nat. Neurosci.* **2,** 422–426
19. Chomczynski, P., and Sacchi, N. (1987) *Anal. Biochem.* **162,** 156–159
20. Kyte J., and Doolittle, R. F. (1982) *J. Mol. Biol.* **157,** 105–132
21. Lesage, F., Reyes, R., Fink, M., Duprat, F., Guillemare, E., and Lazdunski, M. (1996) *EMBO J.* **15,** 6400–6407
22. Jackson, M. B. (1985) *Biophys. J.* **47,** 129–137
23. Horn, R., and Lange, K. (1983) *Biophys. J.* **51,** 43, 207–223
24. Doyle, D. A., Cabral, J. M., Pfuetzner, R. A., Kuo, A., Gulbis, J. M., Cohen, S. L., Chait, B. T., and MacKinnon, R. (1998) *Science* **280,** 69–76
25. Wang, Z. W., Kunkel, M. W., Wei, A., Butler, A., and Salkoff, L. (1999) *Ann. N. Y. Acad. Sci.* **868,** 286–303
26. Leonoudakis, D., Gray, A. T., Winegar, B. D., Kindler, C. H., Harada, M., Taylor, D. M., Chavez, R. A., Forsayeth, J. R., and Yost, C. S. (1998) *J. Neurosci.* **18,** 868–877
27. Kim, Y., Bang, H., and Kim, D. (1999) *Am. J. Physiol.* **277,** H1669–H1678
28. Rajan, S., Wischmeyer, E., Karschin, C., Liu, G. X., Preisig-Müller, R., Daut, J., Karschin, A., Derst, C. (2000) *Pflügers Arch. Eur. J. Physiol.* **439,** R382
29. Kim, D., Fujita, A., Horio, Y., and Kurachi, Y. (1998) *Circ. Res.* **82,** 513–518
30. Fakler, B., Schultz, J. H., Yang, J., Schulte, U., Brändle, U., Zenner, H. P., Jan, L. Y., and Ruppersberg, J. P. (1996) *EMBO J.* **15,** 4093–4099
31. Coulter, K. L., Perier, F., Radeke, C. M., and Vandenberg, C. A. (1995) *Neuron* **15,** 1157–1168
32. Tsai, T. D., Shuck, M. E., Thompson, D. P., Bienkowski, M. J., and Lee, K. S. (1995) *Am. J. Physiol.* **268,** C1173–C1178